Spike shape and synaptic-amplitude distribution interact to set the high-frequency firing-rate response of neuronal populations

Magnus J. E. Richardson*
Warwick Mathematics Institute, University of Warwick, Coventry CV4 7AL, United Kingdom

(Received 30 May 2018; published 10 October 2018)

The dynamics of an ensemble of particles driven out of a potential well, with replacement, by the Poissonian arrival of amplitude-distributed shot noise is examined. A general formula for the high-frequency limit of the escape-rate susceptibility is derived. For certain choices of potential well and amplitude distribution the decay of the high-frequency susceptibility exhibits a nonuniversal exponent. This is a qualitatively different response to that predicted by the diffusion approximation. To provide an example the general framework is applied to a problem of current interest in the biophysics of neuronal voltage dynamics. It is shown that the firing-rate response of neurons to rapidly varying stimuli can be significantly enhanced depending on the ratio between the scale of excitatory postsynaptic potentials and the voltage range over which an action potential initiates. The result is robust to various choices of threshold definition and also to synaptic filtering at physiologically reasonable time scales.

DOI: 10.1103/PhysRevE.98.042405

I. INTRODUCTION

The principal neurons of the neocortex generate spike trains that show considerable variability [1] so that, in the context of a recurrent network, neurons receive a highly fluctuating synaptic drive. The integration of the stochastic synaptic input and subsequent generation of variable spike trains has been studied intensively since the mid-1960s [2–4], initially for simplified models of neurons with a leakless or leaky, ohmic membrane response. A common theoretical approach is to model the fluctuating synaptic input as Gaussian white noise, which is applicable when the incoming drive has high rate, low amplitude, and short temporal correlations. For a leaky integrate-and-fire neuron this results in an Ornsetein-Uhlenbeck process with a threshold-reset mechansism to which the Fokker-Planck formalism can be applied [4,5]. At the single neuron or unconnected population level this allows for the calculation of the instantaneous firing rate, spike-train spectrum [6], and coefficient of variation [7]. For networks of neurons the description afforded by the Fokker-Planck framework allows for mean-field networks to be analyzed and the phase diagram of emergent states derived [8,9].

Isolated synaptic potentials evoked between neocortical pyramidal neurons in quiescent tissue have a log-normal amplitude distribution [10] with mean values in the range of 1–2 mV [11–13]. These amplitudes represent a significant fraction of the potential difference between the rest and threshold. Moreover, because the neuronal voltage is typically just below threshold during network activity [14–16] only a few additional inputs may be required to make the neuron spike. Positive correlations within the presynaptic population will increase the likelihood that inputs occur at similar times, increasing the effective size of the synaptic pulses [17–19]. Conversely, short-term synaptic depression [20,21] will act to reduce subsequent amplitudes in closely timed input on the same afferent fibers. Taken together these experimental results suggest that the synaptic-amplitude distribution in active networks will be a function of the network state and that the Gaussian (or diffusion-limit) approximation of small amplitudes will not be reliable under all circumstances.

Though the majority of studies of stochastic neuronal integration have used the small-amplitude, high-rate diffusion limit, the effect of finite amplitude-distributed drive has been included in models to examine the effect of finite-amplitde inputs on subthreshold voltage fluctuations [22–24], firing properties [25–30] with other population-based approaches extending the analysis to filtered [31] or non-Poissonian input [32,33] for the leaky-integrate and fire model. Recently, there have also been a number of analytical advances: a solution for the steady-state and modulated rate of a leaky integrate-and-fire neuron receiving exponentially distributed excitatory and inhibitory synaptic drive [34] was found, an intriguing connection of that result to the more general solution of a neuron driven by dichotomous noise [35] was demonstrated, and the effect of shot noise in inhibitory networks [36] was analyzed with exact results for a variety of inibitory postsynaptic potential distributions [37].

As well as providing a biophysically more detailed description of synaptic drive than the diffusion approximation, there are significant differences in the response of neurons to finite-amplitude drive. Neurons driven by shot noise respond faster [27] and exhibit qualitatively different response to high-frequency modulations [34]. This is particularly the case for the treatment of modulated inhibition [27,34] because in the diffusion approximation inhibitory fluctuations contribute to the voltage variance which can bring a neuron across threshold, whereas in the shot-noise description it

*Correspondence: magnus.richardson@warwick.ac.uk

is only the excitatory component that can cause an action potential.

The second component of the forward modeling from synaptic-input statistics to neuronal firing patterns is the neuronal response itself. The majority of results for the stochastic integration of synaptic drive, both for Gaussian and shot-noise drive, have been derived with neurons for which the membrane response is linear and ohmic, specifically for the leaky integrate-and-fire (LIF) neuron model (see Refs. [38,39] for a comprehensive early review). Near the threshold for spike initiation, however, the current-voltage relationship is nonlinear due to the activation of the spike-generating sodium current [40]. A variety of nonlinear generalizations of the LIF model have been proposed, with the quadratic IF [41] the most well known of early models. Later, a principled reduction of a detailed, high-dimensional neuron model to a one-variable model suggested that the nonlinear current-voltage relationship should combine a linear term with an exponential nonlinearity near the spike-initiation threshold [42]. It was then shown experimentally that this exponential integrate-and-fire (EIF) model provides an accurate model of the integration properties of neocortical pyramidal cells in layers 2/3, 4, and 5 [43,44] and fast-spiking interneurons [45]. Empirically, the voltage range around threshold over which the spike starts to activate is between $\delta_{\mathrm{T}} = 0.5$ and 1.5 mV. An interesting observation [46] is that the spike-onset sharpness δ_{T} plays a key role in setting the crossover frequency above which populations of EIF neurons respond with decreasing amplitude to modulated Gaussian synaptic drive: the smaller δ_{T}, the higher the cutoff frequency.

Synaptic amplitudes are typically of the order of 1 mV and the experimentally measured spike-onset sharpness has a similar range, so an obvious question is whether there is some interaction between these two extrinsic and intrinsic biophysical quantities that affects neuronal integration—this is the subject of this paper. First, in Sec. II, a general framework for analyzing the high-frequency response of nonlinear IF neurons driven by amplitude-distributed shot noise is developed. In Secs. III and IV it is shown that for populations of EIF neurons the ratio of mean synaptic amplitude and spike-onset sharpness has a qualitative effect on the high-frequency response. In Secs. V and VI the robustness of the results are examined against spike-threshold definition and synaptic-filtering time scale, respectively. The paper closes with a Discussion followed by an Appendix containing technical details of the numerical approaches used. The Julia code [47] used to generate the first three figures is also provided in the Supplemental Material [48].

II. GENERAL RESULT

A population of neurons is considered, each with a state variable v and each receiving independent realizations of a Poissonian shot-noise process $s(t)$ of rate $R(t)$. The dynamics of one of the neurons obeys

$$\frac{dv}{dt} = f(v) + s(t). \tag{1}$$

The Poisson-distributed pulses arrive at times $\{t_k\}$ with each pulse having a positive amplitude a_k independently drawn from a distribution $A(a)$ so that

$$s(t) = \sum_{\{t_k\}} a_k \delta(t - t_k). \tag{2}$$

Hence, on the arrival of a pulse at time t_k, the voltage jumps by a_k. The continuity equation for a population of neurons with an explicit spike, such as for the quadratic or exponential integrate-and-fire model, takes the form

$$\frac{\partial P}{\partial t} + \frac{\partial J}{\partial v} = r\delta(v - v_{re}), \tag{3}$$

where $P(v,t)$ is the probability density, $J(v,t)$ is the flux, and $r(t)$ is the time-dependent firing rate. The Dirac-delta source term handles the voltage reset v_{re} from the sink at threshold v_{th}. We first consider the limit $v_{\mathrm{th}} \to \infty$ and will treat the case of a finite threshold in Sec. V. The flux can be resolved into two components: the first arising from the intrinsic voltage dynamics and the second from the synaptic shot-noise drive J_s

$$J = fP + J_s. \tag{4}$$

In the limit $v \to \infty$ the flux J tends to the ensemble escape rate $r(t)$ and hence

$$P(v,t) \to \frac{r(t)}{f(v)} \tag{5}$$

for high voltages. The shot-noise flux includes jumps that bring the voltage past v from lower values u, so

$$J_s(v,t) = R_s(t) \int_{-\infty}^{v} du\, P(u,t) T(v-u), \tag{6}$$

where $T(v) = \int_v^\infty A(a)da$ is the tail function of the shot-noise amplitude distribution. Note that the large-v behavior of J_s depends on whether the product of the density $P \simeq r(t)/f(u)$ and tail function $T(v-u)$ decreases or grows with u in the integrand in Eq. (6). If the amplitudes are small, as assumed in the standard diffusion approximation, then only the density $P(u)$ near v contributes significantly to the integral; however, if the amplitudes are large then jumps from the entire probability density below v need be accounted for. The coupled integro-differential equations (3)–(6) fully specify the dynamics of the system for an arbitrary rate $R_s(t)$.

A. Steady-state distribution and rate

When the incoming rate is constant $R_s(t) = \bar{R}_s$, the distribution and flux take their steady-state values $\bar{P}$, $\bar{J}_s$. Integration of the continuity equation (3) gives a step function for the total flux $\bar{J}$ which, on insertion into the flux equation (4), gives

$$\bar{r}\theta(v - v_{re}) = f\bar{P} + \bar{J}_s, \tag{7}$$

with the shot-noise flux defined through its equation

$$\bar{J}_s = \bar{R}_s \int_{-\infty}^{v} du\, \bar{P}(u,t) T(v-u) \tag{8}$$

in steady-state form.

B. Limit of high-frequency susceptibility

A sinusoidal modulation of amplitude $\hat{R}_s$ and of frequency $f = \omega/2\pi$ of the presynaptic rate around its steady-state value

$\bar{R}_s$ is now considered. In complex form this can be written

$$R_s(t) = \bar{R}_s + \hat{R}_s e^{i\omega t}. \tag{9}$$

For weak modulation, or for high-frequency modulation in which the response becomes weak, the density will be well approximated by $P(v,t) \simeq \bar{P} + \hat{P}\, e^{i\omega t}$, where $\bar{P}(v)$ is the steady-state density and $\hat{P}(v;\omega)$ is proportional to $\hat{R}_s$. A similar approximation for the flux and firing rate, with analogous notation, can also be made.

The goal of this section is to calculate the high-frequency limit of the modulated firing rate $\hat{r}(\omega)$—this quantity is a direct measure of the susceptibility of the neuronal population to modulated input. The first step is to substitute the modulated density from the flux equation (4) into the continuity equation (3) to give

$$\frac{f}{i\omega}\frac{d\hat{J}}{dv} + \hat{J} = \hat{J}_s. \tag{10}$$

The source term has been dropped: only behavior for $v > v_{\rm re}$ needs to be considered because extracting the asymptotics in the limit $\omega \to \infty$ will require analysis of the density and flux in the limit $v \to \infty$. However, this limit also implies $f(v) \to \infty$ and, because the ratio f/ω appears in Eq. (10), some care is required. To this end the variable $\lambda(v)$ is introduced:

$$\lambda = i\omega \int_v^\infty \frac{dy}{f(y)} \quad \text{so that} \quad \frac{f}{i\omega}\frac{d}{dv} = -\frac{d}{d\lambda}. \tag{11}$$

The transformation has a natural interpretation because the integral above is the escape time starting from a point v outside the potential well. Usefully, the limit $v \to \infty$ corresponds to $\lambda \to 0$, where the modulated flux tends to the modulated escape rate $\hat{J} \to \hat{r}$. We now rewrite Eq. (10) in terms of λ

$$\frac{d\hat{J}}{d\lambda} - \hat{J} = -\hat{J}_s \tag{12}$$

and analytically continue $\hat{J}$ by integrating λ from $0 \to \infty$ to show that $\hat{r}$ is the Laplace transform of $\hat{J}_s$ when expressed in terms of the variable λ

$$\hat{r} = \int_0^\infty d\lambda\, e^{-\lambda} \hat{J}_s(v(\lambda;\omega)). \tag{13}$$

Furthermore, for high frequencies $\hat{J}_s$ becomes proportional to the steady-state shot-noise flux $\bar{J}_s$. This is seen in Eq. (6) evaluated at the weak-modulation level

$$\hat{J}_s = \hat{R}_s \int_{-\infty}^{v} du\, \bar{P}(u) T(v-u) + \bar{R}_s \int_{-\infty}^{v} du\, \hat{P}(u) T(v-u). \tag{14}$$

The second term on the right-hand side becomes less significant at high frequency because from Eq. (3) the modulated density $\hat{P}$ decays as $1/i\omega$ times the flux and rate, which themselves do not grow with frequency. The first term in Eq. (14) is proportional to the steady-state shot-noise flux [Eq. (8)] so that $\hat{J}_s \to \hat{R}_s \bar{J}_s/\bar{R}_s$ in the high-frequency limit. Combining this result with Eq. (13) gives

$$\lim_{\omega\to\infty} \hat{r} = \frac{\hat{R}_s}{\bar{R}_s} \int_0^\infty d\lambda\, e^{-\lambda} \bar{J}_s(v(\lambda;\omega)), \tag{15}$$

where $\bar{J}_s(v(\lambda;\omega))$ is the $v \to \infty$ limit of the steady-state shot-noise flux rewritten in terms of λ. Generally speaking, on substitution of $v(\lambda)$ a series of terms with increasing reciprocal powers of $i\omega$ is found, with the leading-order term giving the high-frequency asymptote. This is the shot-noise extension of an earlier result for Gaussian white noise [49] and is the main result of the current paper: the high-frequency susceptibility of a general class of nonequilibrium escape processes can be written as a Laplace transform of the steady-state shot-noise flux.

III. EIF MODEL WITH TWO COMMON CASES

The results of the previous section are now used to investigate the high-frequency response of the exponential integrate-and-fire (EIF) model neuron [42] to finite-amplitude synaptic drive. This model that has been shown to provide an accurate description of experimental data [43], while at the same time maintaining a good level of mathematical tractability. The dynamics of the model in this context can be written

$$\tau \frac{dv}{dt} = \delta_{\rm T} e^{(v-v_{\rm T})/\delta_{\rm T}} - v + \tau s(t), \tag{16}$$

where the shot-noise process $s(t)$ is defined by Eq. (2). These dynamics are supplemented by a threshold at infinity and reset to $v_{\rm re}$. The intrinsic voltage dynamics are governed by the forcing term

$$f(v) = \frac{1}{\tau}(\delta_{\rm T} e^{(v-v_{\rm T})/\delta_{\rm T}} - v), \tag{17}$$

where τ is the membrane time constant and $\delta_{\rm T} < v_{\rm T}$ are positive parameters that characterize the onset of the action potential or spike. Plots of the force $f(v)$ and the equivalent potential well $-\int^v dv\, f(v)$ are provided in Fig. 1(a). Biophysically, $\delta_{\rm T}$ is related to how rapidly the spike-generating sodium current activates, whereas $v_{\rm T}$ is a measure of the voltage around which this current becomes significant [42]. It can be noted that the leaky-integrate-and-fire model, featuring a linear forcing term, is recovered in the limit $\delta_{\rm T} \to 0$. The lower stable $v_{\rm s}$ and upper unstable $v_{\rm u}$ voltage fixed points $f(v) = 0$,

$$v_{\rm s} = -\delta_T W_0(-e^{-v_{\rm T}/\delta_{\rm T}}), \quad v_{\rm u} = -\delta_{\rm T} W_{-1}(-e^{-v_{\rm T}/\delta_{\rm T}}), \tag{18}$$

can be written [50] in terms of Lambert W functions. For the values $v_{\rm T} = 10$ mV and $\delta_{\rm T} = 0.6$ mV used in the figures the fixed points are $v_{\rm s} \simeq 3.46 \times 10^{-8}$ mV and $v_{\rm u} \simeq 11.8$ mV. The reset $v_{\rm re} = 5$ mV is chosen so that $v_{\rm s} < v_{\rm re} < v_{\rm u}$.

Before going on to consider the effects of different synaptic-amplitude distributions, it is worth calculating the form of the quantity λ given by equation pair (11) for the EIF model. To avoid complicating the later derivations by introducing unnecessary subdominant terms only the exponential term in $f(v) \simeq \delta_{\rm T} e^{-(v-v_{\rm T})/\delta_{\rm T}}/\tau$ is used in equation pair (11). This is because the linear forcing term in Eq. (16) will not contribute significantly in the high-voltage limit. In this approximation λ becomes

$$\lambda = i\omega\tau\, e^{-(v-v_{\rm T})/\delta_T}. \tag{19}$$

This completes the description of the intrinsic, neuronal component of the model. In the remainder of this section two

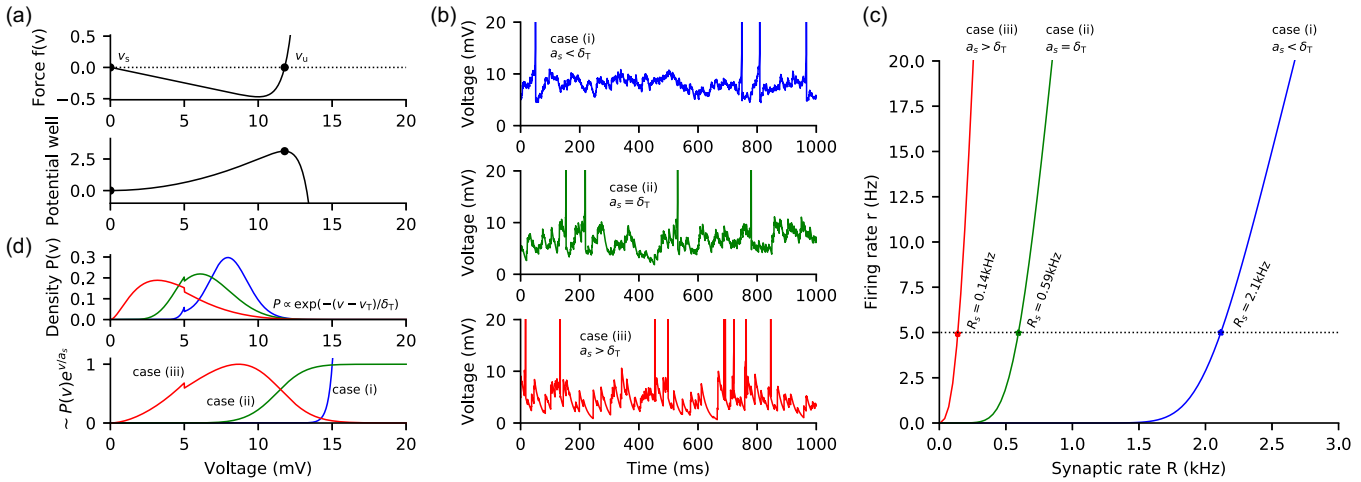

FIG. 1. Steady-state properties of an exponential integrate-and-fire (EIF) neuron driven by a shot-noise process with exponentially distributed amplitudes. (a) Force $f(v)$ given in Eq. (17) and corresponding potential. The stable and unstable fixed points are marked. The $f(v)$ minimum is at v_T and δ_T sets the steepness outside the well. Parameters used are $\tau = 20$ ms, $v_T = 10$ mV, and $\delta_T = 0.6$ mV. (b) Example voltage time courses for three cases (i)–(iii) with small, medium, and large exponentially distributed synaptic amplitudes (mean $a_s = 0.2,\ 0.6,$ and 1.8 mV, respectively). The synaptic rate $\bar{R}_s$ for each case is adjusted so the firing rate is $r = 5$ Hz. (c) Firing rate $\bar{r}$ versus synaptic rate $\bar{R}_s$ for each case with 5 Hz cases marked (symbols). (d) Probability densities $\bar{P}(v)$ corresponding to the examples of panel (b). At voltages $v \gg v_T$ the densities all decay exponentially with scale δ_T [see Eq. (5)]. The synaptic flux $\bar{J}_s$ [Eq. (6)] involves an integral over $\bar{P}(v)\exp(v/a_s)$ and so the behavior of the integrand changes qualitatively with the ratio a_s/δ_T. Other parameters used are $v_{re} = 5$ mV and $v_{th} = 30$ mV. The code generating the figure is provided in the Supplemental Material [48].

common choices for the synaptic-amplitude distribution $A(a)$, that of small and then constant amplitudes, are considered before going on to examine a biophysically motivated choice for $A(a)$ that leads to richer behavior in Sec. IV.

A. Prediction of diffusion approximation

The EIF model driven by stochastic synaptic drive has been studied extensively in the diffusion approximation, under the assumption of high input rate R_s and small synaptic amplitudes a_k, to yield a Gaussian white-noise process. In this limit the tail function $T(a)$ decays sharply and the integral in Eq. (6) depends only locally on P. Performing a Taylor expansion of $P(u)$ around v in Eq. (6) results in

$$J_s = R_s P \int_0^\infty da\, T(a) - R_s \frac{\partial P}{\partial v} \int_0^\infty da\, a\, T(a) + \cdots . \quad (20)$$

From the tail function definition $dT/da = -A(a)$ so it is straightforward to show, using integration by parts, that

$$J_s \simeq R_s \langle a \rangle P - R_s \frac{\langle a^2 \rangle}{2} \frac{\partial P}{\partial v}, \quad (21)$$

where the expansion is truncated at second order (the diffusion approximation) and the angular parentheses denote an average over the distribution $A(a)$. Substitution into Eqs. (3) and (4) yields a Fokker-Planck equation

$$\frac{\partial P}{\partial t} = R_s \frac{\langle a^2 \rangle}{2} \frac{\partial^2 P}{\partial v^2} - \frac{\partial}{\partial v}[(f + R_s \langle a \rangle)P] + r\delta(v - v_{re}). \quad (22)$$

The corresponding high-frequency firing-rate response has already been derived elsewhere [46] as

$$\hat{r}(\omega) \simeq \hat{R}_s \frac{\tau \bar{r}}{i\omega\tau} \left(\frac{\langle a \rangle}{\delta_T} + \frac{\langle a^2 \rangle}{2\delta_T^2} \right), \quad (23)$$

where $\bar{r}$ is the steady-state rate. The prediction of the diffusion approximation for the high-frequency exponent $\hat{r} \sim 1/(i\omega)^\beta$ is therefore $\beta = 1$ and is universal because it is not a function of the parameters of the externally imposed synaptic drive.

B. Fixed synaptic amplitude

The general result [Eq. (15)] derived earlier is now used to go beyond the diffusion approximation by considering fixed, but not necessarily small, synaptic amplitude a_s. For this case the amplitude and tail functions are

$$A(a) = \delta(a - a_s), \quad T(a) = \theta(a_s - a). \quad (24)$$

To use the formula for the high-frequency susceptibility the synaptic flux in the limit of large voltages is required. The form $\bar{P}(v) \simeq \bar{r}\tau\, e^{-(v-v_T)/\delta_T}/\delta_T$ is used for the steady-state density [see Eq. (5)] and, combined with the steplike tail function $T(a)$, the steady-state synaptic flux [Eq. (8)] becomes

$$\bar{J}_s(v) \simeq \bar{R}_s \bar{r} \tau (e^{a_s/\delta_T} - 1) e^{-(v-v_T)/\delta_T} \quad (25)$$

in the high-voltage limit. We now rewrite this in terms of λ using its form in Eq. (19) to give

$$\bar{J}_s(\lambda; \omega) \simeq \bar{R}_s \bar{r} \tau (e^{a_s/\delta_T} - 1) \frac{\lambda}{i\omega\tau}. \quad (26)$$

The steady-state shot-noise flux, now parameterised by λ, can be inserted into the result (Eq. (15)) to give

$$\hat{r} \simeq \hat{R}_s \frac{\bar{r}\tau}{i\omega\tau} (e^{a_s/\delta_T} - 1) \quad (27)$$

in the high-frequency limit. Note that this has the same exponent as the diffusion approximation, and agrees with that approximation up to order a_s^2/δ_T^2, as expected.

IV. EIF WITH EXPONENTIAL AMPLITUDES

In this section the case of synaptic amplitudes drawn from an exponential distribution of mean a_s

$$A(a) = e^{-a/a_s}/a_s, \quad T(a) = e^{-a/a_s} \tag{28}$$

is considered in detail. Though isolated synaptic amplitudes between layer-5 pyramidal neurons can be modeled by a log-normal distribution [10], it should be remembered that in active networks many additional processes will act to deform this distribution, such as short-term synaptic depression and presynaptic correlations. From experience, an exponential tail is a reasonable choice for the synaptic-amplitude distribution neurons receive in an active network. As will be seen, this choice also leads to qualitatively different response properties depending on the relative magnitudes of a_s and the spike-sharpness parameter δ_T.

With an exponential amplitude distribution [34] the integral equation (6) satisfies the differential equation

$$\frac{\partial J_s}{\partial v} + \frac{J_s}{a_s} = R_s P, \tag{29}$$

and so the master equation can be expressed in terms of the coupled differential equations (3) and (29), together with the flux relation of Eq. (4).

A. Steady-state distribution and rate

Equation (7) and the steady-state form of Eq. (29) can be combined to give a first-order differential equation for either the probability density or the shot-noise flux

$$\frac{d\bar{J}_s}{dv} + \bar{J}_s\left(\frac{1}{a_s} + \frac{\bar{R}_s}{f(v)}\right) = \bar{r}\frac{\bar{R}_s}{f(v)}. \tag{30}$$

This equation can be solved analytically; however, the solution is in the form of multiple nested integrals, is not particularly transparent, and is awkward to evaluate numerically. An alternative approach is to directly integrate the differential equations with the boundary conditions included by adapting a numerical scheme [49] developed for diffusion approximations of synaptic drive (see the Appendix for this method and also direct integration of the master equation). Figure 1(b) shows time courses for three cases where the amplitudes satisfy (i) $a_s < \delta_T$, (ii) $a_s = \delta_T$, and (iii) $a_s > \delta_T$, with the synaptic rate R_s adjusted so that each case has a firing rate $r = 5$ Hz. Figure 1(c) shows the steady-state output rate $\bar{r}$ over a range of input synaptic rates $\bar{R}_s$ with steady-state probability densities shown in the upper panel of Fig. 1(d).

B. High-frequency firing-rate response

The general result [Eq. (15)] is now used to derive the high-frequency asymptotics for cases (i)–(iii). To use this formula the steady-state shot-noise flux (6) needs to be derived for each of the three cases. Note first that the tail function $T(v-u)$ grows exponentially with u with scale a_s, whereas in the high-voltage limit the probability density decays exponentially with scale δ_T, because in this limit $P(u) \simeq \bar{r}\tau\, e^{-(u-v_T)/\delta_T}/\delta_T$ [see Eq. (5)]. The product of these growing and decaying exponential terms within the integral for the synaptic flux [Eq. (8)] will have distinct behavior depending on the relative values of a_s and δ_T [see the lower panel of Fig. 1(d)]. For case (i) $a_s < \delta_T$ only the distribution of P at large v is relevant (this case includes the diffusion limit), case (ii) is marginal $a_s = \delta_T$, and for case (iii) where $a_s > \delta_T$ jumps from the bulk of the distribution below v_T will contribute more significantly than local jumps.

To derive an analytical approximation for the high-frequency asymptotics the steady-state synaptic component of the flux $\bar{J}_s(v)$ must be reexpressed as a function of the quantity λ. Because λ is itself a function of $v - v_T$ [see Eq. (19)] it makes sense to write the leading-order forms of $\bar{J}_s(v)$ in the limit of high voltage as functions of $v - v_T$ before substituting for λ. This requires approximating the integral form for $\bar{J}_s(v)$ in Eq. (8) and making use of the high-voltage limit $\bar{P}(v) \simeq \bar{r}\tau\, e^{-(v-v_T)/\delta_T}/\delta_T$. The derivations of these leading-order forms for each case are now presented.

Case (i). When $a_s < \delta_T$ the product of the steady-state probability density and amplitude tail function grows exponentially with u in the integrand of Eq. (8) for $\bar{J}_s$ [see Fig. 1(d), blue curve] so $\bar{J}_s$ can be approximated by

$$\bar{J}_s(v) \simeq R_s r\tau \int_{-\infty}^{v} \frac{du}{\delta_T} e^{-(u-v_T)/\delta_T - (v-u)/a_s}, \tag{31}$$

which can be integrated to give

$$J_s(v) \simeq \frac{R_s r\tau a_s}{\delta_T - a_s} e^{-(v-v_T)/\delta_T}. \tag{32}$$

Case (ii). For the marginal case where $a_s = \delta_T$ the synaptic flux is

$$\bar{J}_s(v) = \bar{R}_s e^{-(v-v_T)/\delta_T} \int_{-\infty}^{v} du\, \bar{P}(u) e^{(u-v_T)/a_s}. \tag{33}$$

When v is large the decaying exponential in $P(u)$ exactly matches the exponentially growing shot-noise amplitude, so the integrand tends to a constant [Fig. 2(d), green curve] and the integral grows linearly as $\bar{r}\tau v/\delta_T$. The integral in the previous equation can be rewritten as

$$\bar{r}\tau\frac{(v - v_s)}{\delta_T} + \int_{v_s}^{v} du\left(\bar{P}(u)e^{(u-v_T)/a_s} - \frac{\bar{r}\tau}{\delta_T}\right), \tag{34}$$

which is exact; however, a good approximation is found by setting the upper bound of the integral at infinity because there is little contribution for $v \gg v_T$. The steady-state shot-noise flux for the marginal case (ii) in the high-voltage limit can therefore be approximated by

$$\bar{J}_s(v) \simeq \bar{R}_s\bar{r}\tau\, e^{-(v-v_T)/\delta_T}\left(\frac{(v - v_T)}{\delta_T} + \log(\kappa)\right), \tag{35}$$

where the v-independent component

$$\log(\kappa) = \frac{(v_T - v_s)}{\delta_T} + \int_{v_s}^{\infty} \frac{du}{\delta_T}\left(\frac{\delta_T\bar{P}(u)}{\bar{r}\tau}e^{(u-v_T)/a_s} - 1\right) \tag{36}$$

has been written in this way in anticipation of it being combined with other logarithms in the resulting form for the firing-rate modulation.

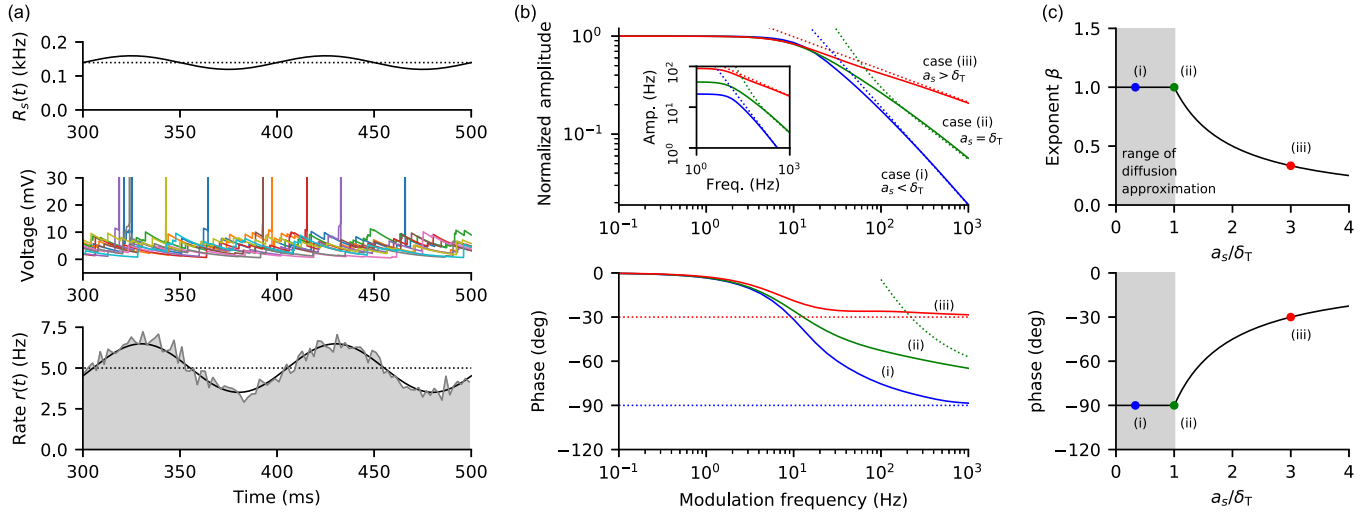

FIG. 2. Response of a population of shot-noise driven EIF neurons to modulated synaptic rate. (a) Weak sinusoidal modulation [Eq. (9)] of the synaptic rate $R_s(t)$ (top panel) induces sinusoidal modulation of the population (simulations, middle panel) firing rate $r(t)$ around its steady state (histogram compared to theory, bottom panel). The amplitude and phase shift of the firing-rate response are frequency dependent. (b) Amplitude (top) and phase (bottom) of $\hat{r}$ versus modulation frequency [cases (i)–(iii)] around the 5 Hz steady state shown in Figs. 1(b)–1(d). The amplitude has been normalized to be unity at low frequencies and asymptotic forms [dashed lines: Eqs. (42)–(44)] are also plotted. Case (iii) amplitude is ∼50 times higher than case (i) at 1000 Hz modulation. The inset shows the unnormalized amplitude ($\hat{R}_s = 1$ kHz). (c) The high-frequency exponent as a function of the ratio of the mean synaptic amplitude a_s to the spike parameter δ_T. At high frequencies $\hat{r} \sim 1/(i\omega\tau)^\beta$ with the diffusion approximation $\beta = 1$ only valid for small jumps $a_s < \delta_T$. Model parameters are the same as Fig. 1. The code generating the figure is provided in the Supplemental Material [48].

Case (iii). For the case where $a_s > \delta_T$ the synaptic flux is dominated by jumps from the bulk of the distribution so that we extend the integral in Eq. (8) to infinity and approximate $\bar{J}_s$ as

$$\bar{J}_s(v) \simeq \bar{R}_s e^{-(v-v_T)/a_s} \int_{-\infty}^{\infty} du\, \bar{P}(u) e^{(u-v_T)/a_s}. \tag{37}$$

This can be integrated to give

$$\bar{J}_s(v) \simeq \bar{R}_s \bar{r}\tau\, e^{-(v-v_T)/a_s} I_s, \tag{38}$$

where $I_s = \int_{-\infty}^{\infty} du\, e^{(u-v_T)/a_s} \bar{P}(u)/\bar{r}\tau$ is over a steady-state quantity and independent of v. Note that in this case the denominator of the exponential in Eq. (38) is a_s rather than δ_T, as was the case for cases (i) and (ii).

The voltage-dependent forms for the steady-state synaptic flux $\bar{J}_s(v)$ for the three cases given in Eqs. (32), (35), and (38) can now be used to derive the λ-dependent forms by substituting for $v - v_T$ using Eq. (19). This results in

$$\bar{J}_s \simeq \frac{\bar{R}_s \bar{r}\tau a_s}{\delta_T - a_s} \frac{\lambda}{i\omega\tau}, \tag{39}$$

$$\bar{J}_s \simeq \bar{R}_s \bar{r}\tau \frac{\lambda}{i\omega\tau} \log\left(\frac{i\omega\tau\kappa}{\lambda}\right), \tag{40}$$

$$\bar{J}_s \simeq \bar{R}_s \bar{r}\tau \left(\frac{\lambda}{i\omega\tau}\right)^{\frac{\delta_T}{a_s}} I_s \tag{41}$$

to leading order in a high-frequency expansion for cases (i)–(iii), respectively. Note that because of the argument of the exponential in case (iii) Eq. (38) fractional powers of λ and ω are generated.

These forms can then be integrated in the Laplace-transform equation (15) to finally yield the desired asymptotics:

$$\hat{r}(\omega) \simeq \hat{R}_s \frac{\bar{r}\tau}{i\omega\tau} \frac{a_s}{\delta_T - a_s} \quad \text{for } a_s < \delta_T, \tag{42}$$

$$\hat{r}(\omega) \simeq \hat{R}_s \frac{\bar{r}\tau}{i\omega\tau} \log(i\omega\tau\tilde{\kappa}) \quad \text{for } a_s = \delta_T, \tag{43}$$

$$\hat{r}(\omega) \simeq \hat{R}_s \frac{\bar{r}\tau I_s}{(i\omega\tau)^{\delta_T/a_s}} \Gamma\left(\frac{\delta_T}{a_s} + 1\right) \quad \text{for } a_s > \delta_T, \tag{44}$$

where $\tilde{\kappa} = \kappa\, e^{\gamma - 1}$ with $\gamma \simeq 0.5772$ (the Euler-Mascheroni constant) and where $\Gamma(m)$ is the standard Gamma function. The high-frequency susceptibility $1/(i\omega)^\beta$ exponent β is therefore not universal: it takes the synaptic-input independent value $\beta = 1$ predicted by the diffusion approximation only for small synaptic amplitudes $a_s < \delta_T$, whereas when $a_s > \delta_T$ the exponent $\beta = \delta_T/a_s$ is a function of the synaptic amplitude distribution. The latter condition is relevant experimentally as δ_T can be less than 1 mV [43] and the mean synaptic amplitude, even in the absence of correlations, is of the order of 1.5 mV between neocortical layer-5 pyramidal cells [11]. The asymptotic results are plotted [Fig. 2(b) with a numerical solution of the master equation (see the Appendix). The exponent as a function of the ratio a_s/δ_T is plotted in Fig. 2(c). Note that these asymptotics are different to those for the shot-noise driven leaky-integrate-and-fire model [34] because the limits $\delta_T \to 0$ and $\omega \to \infty$ do not commute.

C. Rapid response in the time domain

The same phenomenon can be seen in the time domain. Defining the susceptibility $\hat{\chi}(w) = \hat{r}(w)/\hat{R}$, the response to

a delta-function synaptic-rate impulse $R_s(t) = \bar{R}_s + \delta(t)$ is written $r(t) = \bar{r} + \chi(t)$, where $\bar{r}$ is the steady-state rate and $\chi(t)$ is the inverse Fourier transform $\int d\omega\, \hat{\chi}\, e^{i\omega t}/2\pi$ of the susceptibility. A convenient approximation extrapolates between low- and high-frequency limits

$$\hat{\chi}(\omega) \simeq \frac{c_\infty}{(i\omega\tau + c_0)^\beta}. \tag{45}$$

The quantity c_∞ is the prefactor of the $1/(i\omega\tau)^\beta$ terms in Eq. (42) or (44) without the $\hat{R}_s$ factors, and $c_0^\beta = c_\infty/\hat{\chi}(0)$. The low-frequency limit of the susceptibility $\hat{\chi}(0)$ is the gradient $d\bar{r}/d\bar{R}_s$ of the steady-state rate curve [Fig. 1(c)]. The inverse transform of Eq. (45) provides the following approximation:

$$\chi(t) \simeq \frac{1}{\tau}\frac{c_\infty}{\Gamma(\beta)}\left(\frac{\tau}{t}\right)^{1-\beta} e^{-c_0 t/\tau}. \tag{46}$$

For case (i) where $\beta = 1$ the response is finite at $t = 0$ (previously shown using the diffusion approximation [46]) and equal to $\bar{r}a_s/(\delta_T - a_s)$. However, for case (iii) there is a power law $\bar{r}I_s\beta(\tau/t)^{1-\beta}$ that diverges at early times. Hence neuronal populations receiving large-amplitude low-rate stimuli respond faster to rapid changes in synaptic rate than those receiving high-rate low-amplitude synaptic drive. This increased responsiveness is demonstrated for a variety of modulated synaptic rates $R(t)$ in Figs. 3(a)–3(c) through numerical solution of the full master equation (see the Appendix for details).

V. EIF WITH FINITE SPIKE THRESHOLD

In this and the next section the robustness of the result of Sec. IV is examined. Thus far the high-frequency asymptotics were derived under the condition of an infinite spike threshold $v_{\rm th}$, which is the voltage at which a spike is registered and the voltage subsequently reset to $v_{\rm re}$. It is relevant to ask what happens if this condition is relaxed and a finite threshold for registering a spike is chosen, as would be the case experimentally. It will now be shown that when the threshold is finite the response to input modulation still behaves as if the threshold was infinite, as long as the modulation frequency is below some crossover value; above the crossover the response to modulation tends to a constant. However, the crossover frequency grows exponentially with $v_{\rm th}$ and so the results derived in the main text, which used an infinite threshold, remain correct for biophysical parameter choices.

The continuity equation at the level of the amplitudes of the modulated parameters is

$$i\omega\hat{P} + \frac{\partial\hat{J}}{\partial v} = \hat{r}\delta(v - v_{\rm re}) - \hat{r}\delta(v - v_{\rm th}). \tag{47}$$

In the limit $\omega \to \infty$ it must be that $\hat{P} \to 0$ because neither the modulated flux $\hat{J}$ nor the rates diverge. The implication in the corresponding flux equation evaluated at threshold $v_{\rm th}$

$$\hat{J}(v_{\rm th}) = f(v_{\rm th})\hat{P}(v_{\rm th}) + \hat{J}_s(v_{\rm th}) \tag{48}$$

is that the contribution of $\hat{P}$ will ultimately vanish in the high-frequency limit. Because $\hat{J}(v_{\rm th}) = \hat{r}$ this leads to the finite-

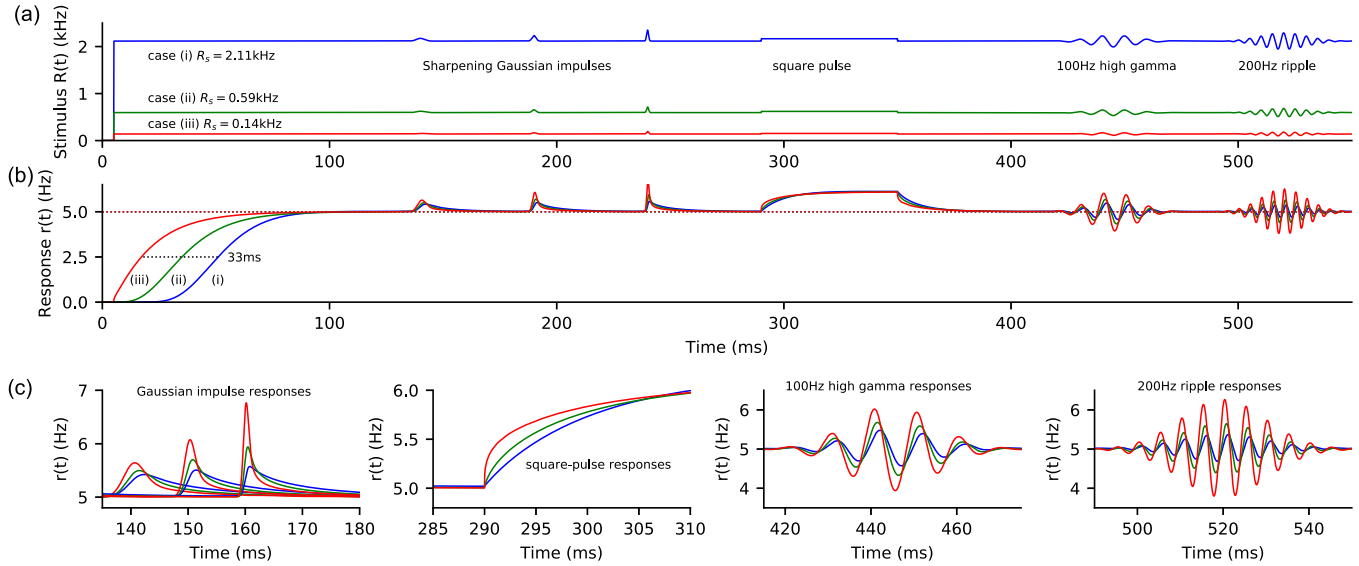

FIG. 3. Populations of EIF neurons receiving large-amplitude low-rate synaptic drive react faster and stronger to transients than those receiving small-amplitude high-rate drive. (a) The stimulus $R_s(t)$ comprises constant-area Gaussian impulses with increasing temporal sharpness, a square-pulse current, and two chirps at 100 Hz and 200 Hz all sitting on a background stimulation that results in a 5 Hz firing rate [see Fig. 1 for the three cases (i)–(iii)]. (b) The firing-rate response for the three cases. Note that the large-amplitude, low-rate case (iii) response is much faster (a 33 ms difference at the midvalue) than the diffusionlike case (i) to the onset of the stimulation. (c) Details of the firing-rate response as marked. The responses to sharpening, constant-area Gaussian rate impulses converge to the time-domain susceptibility [see Eq. (46)]: case (i) remains finite, whereas cases (ii) and (iii) diverge at early times for increasingly sharp impulses. For square-pulse stimuli case (iii) responds fastest to the onset (infinite gradient at onset) and, similarly, for oscillating waveforms, where for the 200 Hz chirp case (iii) response is four times greater than that of case (i). Neuronal parameters are the same as Fig. 1 and the stimulus parameters are given in the Appendix. The code generating the figure is provided in the Supplemental Material [48].

threshold, infinite-frequency result

$$\lim_{\omega\to\infty} \hat{r} = \hat{J}_s(v_{\rm th}) = \frac{\hat{R}_s}{R_s}\bar{J}_s(v_{\rm th}), \tag{49}$$

where the proportionality between $\hat{J}_s$ and $\bar{J}_s$ at high frequency has been used [see discussion around Eq. (14)]. Hence, for a finite threshold, the infinite-frequency limit tends to a constant—this is qualitatively different to the infinite-threshold results for cases (i)–(iii) derived in the main text for which $\hat{r}$ exhibited power-law decays in frequency. However, two aspects of this result should be noted. The first is that the constant response given in Eq. (49) above decreases exponentially with increasing $v_{\rm th}$ by virtue of the voltage dependence of $\bar{J}_s(v)$ [see Eqs. (32), (35), and (38)]. The second aspect is that the result just derived required that the term $f(v_{\rm th})\hat{P}(v_{\rm th})$ in the modulated flux equation can be neglected at increasing frequency. However, the prefactor $f(v_{\rm th})$ is exponentially large in the threshold $v_{\rm th}$ and so the frequency scale above which this term can be safely neglected grows very rapidly with $v_{\rm th}$. There is therefore a crossover frequency below which the infinite-threshold, power-law decay results are valid and above which the finite-threshold infinite-frequency result begins to dominate.

Crossover frequency dependence on $v_{\rm th}$

The crossover frequency can be found by extending the general result in Sec. II to finite threshold. We start with Eqs. (10) and (11), but use a modified definition of λ,

$$\lambda = i\omega\int_{v}^{v_{\rm th}} \frac{dy}{f(y)}, \tag{50}$$

with the upper limit at $v_{\rm th}$ rather than infinity. The rest of the derivation follows just like the infinite-threshold case resulting in Eq. (15) as before. For moderate thresholds the integral form for λ in Eq. (50) for the EIF model is well approximated by

$$\lambda \simeq i\omega\tau\, e^{-(v-v_{\rm T})/\delta_{\rm T}} - i\omega\tau\, e^{-(v_{\rm th}-v_{\rm T})/\delta_{\rm T}}, \tag{51}$$

which includes an additional term to that in Eq. (19). It is this term that generates the constant response for finite thresholds. However, this term is negligible for low frequencies or high thresholds, in which case the infinite-threshold result holds. A crossover frequency $w_c = 2\pi F_c$ can therefore be found

$$F_c \simeq \frac{1}{2\pi\tau} e^{(v_{\rm th}-v_{\rm T})/\delta_{\rm T}} \tag{52}$$

that grows exponentially with $v_{\rm th}$. More generally, this can be written as

$$F_c = \frac{1}{2\pi\mathcal{T}_{\rm th}}, \quad \text{with } \mathcal{T}_{\rm th} = \int_{v_{\rm th}}^{\infty} \frac{dv}{f(v)}, \tag{53}$$

where $\mathcal{T}_{\rm th}$ would have been the time taken to go from threshold to infinity. The spike threshold only needs to be a few $\delta_{\rm T}$'s above $v_{\rm T}$ (or, more accurately, the unstable fixed point $v_{\rm u}$, which is close in value to $v_{\rm T}$) for the crossover frequency to be sufficiently high that the infinite-threshold power-law asymptotics dominates over all biologically reasonable modulation frequencies. These results are illustrated in Fig. 4 for finite thresholds at $v_{\rm th} = 12,\ 13$, and 14 mV. Figure 4(a) shows the exponential EIF forcing term $f(v)$ and crossover frequency [Eq. (53)] as an inset. Though the constant asymptotics can be clearly seen for $v_{\rm th} = 12$ mV with a crossover at ∼125 Hz [first 4(b) panel], this threshold is just 0.3 mV above the unstable fixed point. Increasing the threshold by 1 mV moves the crossover frequency to ∼1000 Hz [middle 4(b) panel] and increasing by a further 1 mV to 2.3 mV above the unstable fixed point pushes the crossover to above 6000 Hz [last 4(b) panel]. Thus for any reasonable definition of the spike threshold $v_{\rm th}$, the power-law decays in frequency derived in Sec. IV remain valid.

VI. EIF WITH SYNAPTIC FILTERING

Finally, a dynamical feature of synaptic drive that has not been considered in the theoretical treatment thus far is the effect of synaptic filtering due to the finite closing time of the excitatory synaptic channels. This filtering can be accounted for by including a dynamics for the synaptic drive in the

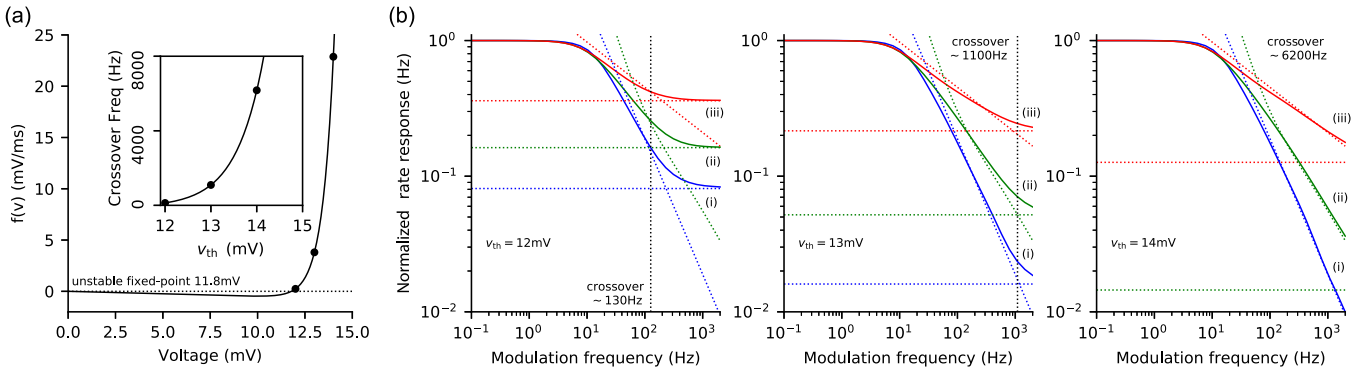

FIG. 4. Effect of a low spike threshold on the modeled high-frequency response. (a) The forcing term $f(v)$ and crossover frequency (inset) given by Eq. (53). Spike threshold $v_{\rm th} = 12,\ 13$, and 14 mV are marked with symbols. (b) Firing-rate response for these three thresholds (as marked) together with infinite-threshold asymptotics [Eqs. (42)–(44)] and the corresponding finite-threshold high-frequency constant asymptotics [Eq. (49); dotted horizontal lines] for each of the three cases (i)–(iii) as marked. The crossover frequency (vertical dotted line) between the power-law asymptotics seen for an infinite threshold (dashed lines) and the constant asymptotes (horizontal dotted lines) increases very rapidly (exponentially) with threshold $v_{\rm th}$. Parameters are the same as for Fig. 1 unless marked.

voltage equation (1) such that $s(t)$ is now governed by the equation

$$\tau_s \frac{ds}{dt} = -s + \sum_{\{t_k\}} a_k \delta(t - t_k), \tag{54}$$

where τ_s is the time scale of the synaptic filtering and a_k is drawn from an exponential distribution as before. Note that in the limit $\tau_s \to 0$ the case of white shot noise [Eq. (2)] is recovered. Away from the region where the spike is generated, this filtered synaptic drive gives excitatory postsynaptic potentials of the classical two-exponential form, with τ_s setting the time scale of the rise and τ the decay

$$v(t) = a_k \frac{\tau}{(\tau - \tau_s)} (e^{-t/\tau} - e^{-t/\tau_s}) \tag{55}$$

for an isolated input and $t > 0$. Experimentally, the time scale τ_s for fast excitatory synaptic conductances are typically quoted as having a mean around 1.7 ms [51] and being in the range 1.3–2 ms [52] (though dendritic filtering can increase the spread of the effective time constant to 2.9 ms $\pm$ 2.3 ms [11]).

An analytical treatment of the high-frequency asymptotics for filtered shot noise is beyond the scope of the current paper; however, it is straightforward to integrate the stochastic equations (16) and (54) and extract the amplitude response for a reasonable range of frequencies. In the three panels of Fig. 5(a) the steady-state rate for cases (i)–(iii) are plotted, each for $\tau_s = 0,\ 1,\ 2,$ and 3 ms. The modulation will again be compared around a steady-state firing rate of 5 Hz and the corresponding incoming rates $\bar{R}_s$ for each case (i)–(iii) and τ_s values were extracted numerically (values given in figure panels). In the four Fig. 5(b) panels, the modulation amplitudes measured from simulations are plotted for the different τ_s values. In the first panel the $\tau_s = 0$ ms simulations are compared to the numerical solution of the master equation [identical to Fig. 2(b)]. For the Fig. 5(b) panels corresponding to $\tau_s = 1,\ 2,$ and 3 a heuristic fit

$$\hat{r}_{\tau_s} \sim \frac{\hat{r}_0}{\sqrt{1 + (\omega\tau_s)^2}} \tag{56}$$

equivalent to a further filtering of the white-Poissonian $\hat{r}_0$ numerical solution of the first panel is plotted for comparison. This heuristic result gives a reasonable indication of the behavior for intermediate frequencies, though at higher frequencies the modulation appears to be further suppressed (compare, for example, the red symbols and red curve in the second panel above for frequencies 300 Hz).

To demonstrate that the stronger high-frequency firing-rate response for case (iii) over case (i) persists in the presence of synaptic filtering, the amplitude ratio of case (iii) to case (i) is plotted for the four different time constants τ_s in Fig. 5(c). The solid line is the ratio of the numerical solution of the master equation for $\tau_s = 0$ ms. Note that the heuristic form gives the same curve for $\tau_s \neq 0$ because the τ_s-dependent factors common to cases (i) and (iii) cancel. The large-frequency limit of the solid line is given by the ratio of Eqs. (44) and (42) and for high frequencies grows as $(\omega\tau)^{1-\delta_T/a_s}$, where a_s is the case (iii) mean amplitude. The ratio of the cases (iii)/(i) simulational points (red divided by blue) from Fig. 5(b) panels are plotted all together in Fig. 5(c) for the four cases up until a frequency where the corresponding case (i) was less than 2% of the low-frequency limit [dashed lines in Fig. 5(b) panels]. As can be seen, the increased responsiveness is apparent even in the case of synaptic filtering. It becomes increasingly

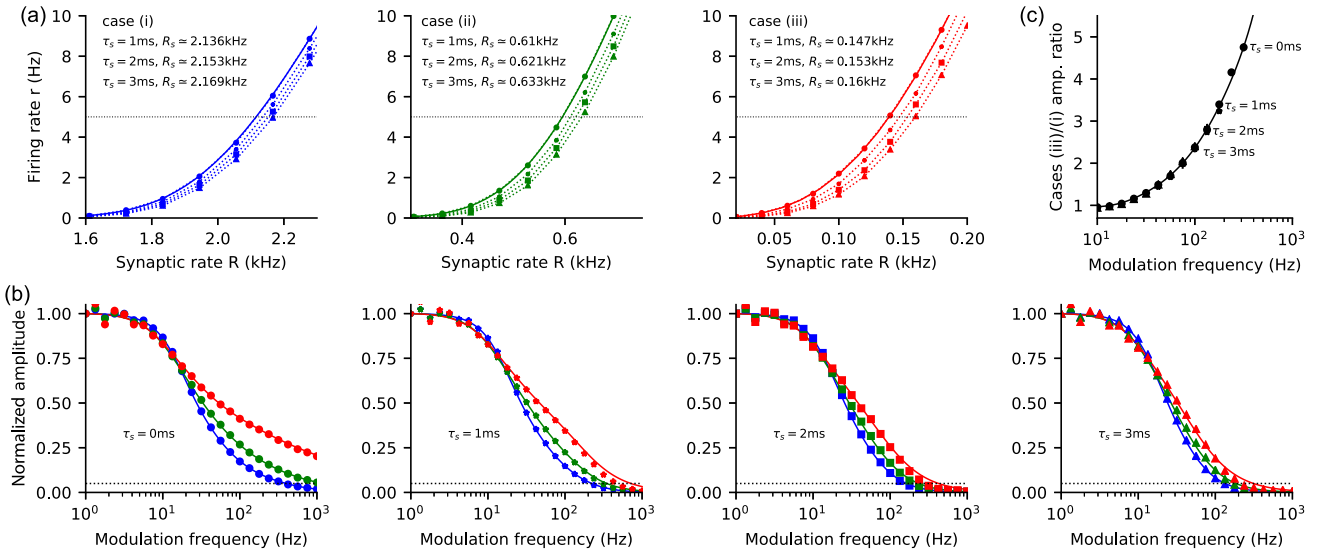

FIG. 5. Effect of synaptically filtered shot noise. (a) Steady-state rates with one panel for cases (i), (ii), and (iii) in blue, green, and red, respectively. The three curves in each panel are for $\tau_s = 0,\ 1,\ 2,$ and 3 ms (circle, star, square, and triangle symbols). The synaptic rates R for 5 Hz are given in the panels. (b) Amplitude of the rate modulation comparing cases (i)–(iii) for four different time constants as marked for the four panels. Simulations are in symbols and heuristic theory [Eq. (56)] lines [color and symbol convention as for (a) panels]. Note the stronger suppression of the high frequencies as τ_s increases. (c) Amplitude ratio between case (iii) and case (i) for synaptic time constants. The increased responsiveness of $a_s > \delta_T$ [case (iii)] to $a_s < \delta_T$ [case (i)] is present to at least 100 Hz even when there is synaptic filtering: simulation [symbols for $\tau_s = 0,\ 1,\ 2,$ and 3 ms with same convention as (a)] and the line is the ratio case (iii)/(i) heuristic theory [Eq. (56)], which is the same for each synaptic time constant (see accompanying text).

difficult to extract the ratio for higher frequencies because the response of case (i) is so strongly suppressed by the synaptic filtering. This region is unlikely to be physiologically relevant, but in the interests of full disclosure it should be noted that for higher frequencies the ratio saturates and appears to decrease.

VII. DISCUSSION

This paper investigated how synaptic-amplitude distributions and intrinsic spike-generating nonlinearities interact to set the high-frequency response properties of neurons. The central theoretical result [Eq. (15)] gives the asymptotic dynamical response in terms of a Laplace transform of the steady-state shot-noise flux. The result is fairly general in that it is applicable to any one-dimensional, nonlinear integrate-and-fire model driven by Poissonian shot noise with arbitrary synaptic amplitude distribution. It can be noted that the result is qualitatively unchanged in the presence of inhibition because the high-frequency response is still expressible as a Laplace transform of the steady-state excitatory flux only.

As an example, the result was used to demonstrate that the firing-rate response of a population of EIF neurons driven by exponentially distributed shot noise is nonuniversal because the high-frequency exponent depends on the mean synaptic amplitude a_s. The diffusion approximation [42,46] relevant in the limit of small a_s predicts a high-frequency rate response that decays with the reciprocal of frequency. The analysis here demonstrates that below a critical value $a_s < \delta_\mathrm{T}$ the prediction of the diffusion approximation is correct and the high-frequency response $1/\omega^\beta$ is universal in that $\beta = 1$ and is independent of the external synaptic drive. However, for mean amplitudes larger than the spike-onset sharpness $a_s > \delta_\mathrm{T}$ the exponent is nonuniversal and dependent on the synaptic amplitude distribution $\beta = \delta_\mathrm{T}/a_s$. These results were shown to be robust to the definition of the spike threshold and, importantly, to synaptic filtering at physiological scales. Though beyond the scope of the current paper the results are also robust against the inclusion of inhibition (as discussed above), an absolute refractory period [this merely modifies the steady-state rate in Eqs. (42)–(44)], and the effects of synaptic conductance (these are weak for excitation due to the relatively high reversal potential).

How spike sharpness determines neuronal response properties [53] has recently come under intense theoretical and experimental scrutiny [54–59]. Modeling studies [46,56,60,61] have shown how the spike-onset sharpness δ_T sets the high-frequency cutoff. However, this effect is distinct to that stemming from the interaction between spike-onset sharpness and the synaptic amplitude distribution highlighted in this paper. Spike-onset sharpness δ_T is an intrinsic property of the cell and largely static, whereas the effective synaptic amplitude distribution is affected by changes in the nature of the activity in the presynaptic network.

Experimental investigations into the high-frequency response properties of neurons typically involved Gaussian input [54,55,57,59,61] or Poissonian input but with modulation via an additional sinusoidal current [58]. These experimental paradigms are distinct from the scenario considered here in which a Poissonian input rate is modulated and synaptic amplitudes are drawn from a distribution. I am unaware of existing experimental studies of the firing-rate susceptibility under these conditions; however, such experiments should be relatively straightforward to perform and would provide an empirical test of the theoretical predictions in this paper.

ACKNOWLEDGMENTS

I would like to thank Nicolas Brunel and Benjamin Lindner for their useful comments on an earlier version of this manuscript.

APPENDIX: NUMERICAL METHODS

Numerical solutions of the system are complicated by the zero in $f(v)$ at the unstable fixed point and the exponential decay of $f(v)$ for large v: this is particularly the case for the computation of high-frequency properties. A number of approaches are used including direct solution of the steady-state rate and linear response, as well as a full solution of the shot-noise master equation in a transformed coordinate system.

1. Steady-state rate and density

It is straightforward to adapt the threshold integration method [49], originally derived for diffusion processes, to the case of shot-noise input. This involves rescaling the density and fluxes by the steady-state rate $\bar{r}$, for example, $\bar{P} = \bar{r}\,\bar{p}$ with analogous definitions for $\bar{J}$ and $\bar{J}_s$. Equation (29) for the synaptic flux can be rearranged

$$\frac{d\bar{J}_s}{dv} + \bar{J}_s\left(\frac{1}{a_s} + \frac{\bar{R}_s}{f}\right) = \frac{\bar{R}_s}{f}\theta(v - v_\mathrm{re}), \tag{A1}$$

where Eq. (4), which gives the density in terms of the fluxes $\bar{p} = (\bar{J} - \bar{J}_s)/f(v)$, has been used and from the continuity equation (3) the scaled steady-state flux is simply $\bar{J} = \theta(v - v_\mathrm{re})$. Equation (A1) can be solved analytically or numerically by integrating up from $v_\mathrm{u} \to v_\mathrm{th}$ (where v_th is sufficiently high that its value does not affect the result) and then down from $v_\mathrm{u} \to v_\mathrm{s}$. Note that $\bar{J} = \bar{J}_s = 1$ at v_u provides the initial conditions. This also implies the scaled density at the unstable fixed point is

$$\bar{p}(v_\mathrm{u}) = \frac{1}{a_s[\bar{R}_s + f'(v_\mathrm{u})]}, \tag{A2}$$

which is found by taking the derivative of Eq. (4) and substituting for the derivative of $\bar{J}_s$ using Eq. (A1). Finally, the steady-state firing rate $\bar{r}$ is recovered by noting $\bar{P}$ integrates to 1 so that $\bar{p}$ integrates to $1/\bar{r}$. This method was used to generate the figure panels 1(c) and 1(d).

2. Rate response to modulated synaptic drive

At the linear level of the response to weak harmonic modulations in the incoming synaptic drive the continuity equation (3) and synaptic flux equation (29) result in two first-order differential equations linking $\hat{J}$ and $\hat{J}_s$,

$$\frac{d\hat{J}}{dv} + i\omega\frac{\hat{J}}{f} - i\omega\frac{\hat{J}_s}{f} = \hat{r}\delta(v - v_{re}), \tag{A3}$$

$$\frac{d\hat{J}_s}{dv} + \hat{J}_s\left(\frac{1}{a_s} + \frac{\bar{R}_s}{f}\right) - \bar{R}_s\frac{\hat{J}}{f} = \hat{R}_s\bar{P}, \tag{A4}$$

where $\bar{P}$ can be found from the solution to (A1) and the relation $\hat{P} = (\hat{J} - \hat{J}_s)/f(v)$ has been used. Note that this relation also implies that at the unstable fixed point $\hat{J}(v_u) = \hat{J}_s(v_u)$. This system of coupled differential equations has two inhomogeneous terms: one proportional to $\hat{r}$ the other proportional to $\hat{R}$. A convenient method for numerical solution, therefore, is to separate the full solution into two independent components each proportional to one of the inhomogeneous terms:

$$\hat{J} = \hat{r}\hat{\jmath}^r + \hat{R}_s\hat{\jmath}^R, \quad \hat{J}_s = \hat{r}\hat{\jmath}_s^r + \hat{R}_s\hat{\jmath}_s^R. \tag{A5}$$

These two components can be solved in much the same way as was the steady state and then combined to yield $\hat{r}$ [see, for example, Fig. 2(b)] as is now described.

Step 1. The solution component that satisfies the inhomogeneous term in Eq. (A3) involving the output rate $\hat{r}$ obeys the equation pair

$$\frac{d\hat{\jmath}^r}{dv} + i\omega\frac{\hat{\jmath}^r}{f} - i\omega\frac{\hat{\jmath}_s^r}{f} = \delta(v - v_{re}), \tag{A6}$$

$$\frac{d\hat{\jmath}_s^r}{dv} + \hat{\jmath}_s^r\left(\frac{1}{a_s} + \frac{\bar{R}_s}{f}\right) - \bar{R}_s\frac{\hat{\jmath}^r}{f} = 0. \tag{A7}$$

At the unstable fixed point $\hat{\jmath}^r(v_u) = \hat{\jmath}_s^r(v_u)$ but, unlike for the steady-state case, this value at v_u is not known *a priori*. However, the value of the modulated flux $\hat{\jmath}^r$ at threshold v_{th} is known and equal to 1 (because $\hat{r}$ has been scaled out). The strategy is therefore to integrate equation pair (A6),(A7) from v_u with initial conditions for $(\hat{\jmath}^r, \hat{\jmath}_s^r)$ of (1,1) and then divide through both fluxes by $\hat{\jmath}^r(v_{th})$. With the values now known at v_u the equation pair (A6),(A7) is integrated down from $v_u \to v_s$. This completes the solution for the component that is proportional to $\hat{r}$.

Step 2. The component that addresses the inhomogeneous term proportional to $\hat{R}_s$ obeys the equations

$$\frac{d\hat{\jmath}^R}{dv} + i\omega\frac{\hat{\jmath}^R}{f} - i\omega\frac{\hat{\jmath}_s^R}{f} = 0, \tag{A8}$$

$$\frac{d\hat{\jmath}_s^R}{dv} + \hat{\jmath}_s^R\left(\frac{1}{a_s} + \frac{\bar{R}_s}{f}\right) - \bar{R}_s\frac{\hat{\jmath}^R}{f} = \bar{P}, \tag{A9}$$

where again we have $\hat{\jmath}^R(v_u) = \hat{\jmath}_s^R(v_u)$ at a value that is not known *a priori*. In this case we will use the result that at threshold $\hat{\jmath}^R = 0$, because the full flux is carried by the $\hat{\jmath}^r$ term. Let's write the solution for $v > v_u$ as the mix

$$\hat{\jmath}^R(v) = \hat{\jmath}^R(v;0) + \kappa\hat{\jmath}^r(v;1), \tag{A10}$$

with a similar definition for $\hat{\jmath}_s^R(v)$ with the same κ. Here $\hat{\jmath}^R(v;0)$ comes from the solution to equation pair (A8),(A9) for $v > v_u$ with initial conditions at v_u of (0,0). The term, $\hat{\jmath}^r(v;1)$, comes from the solution to equation pair (A6),(A7) for $v > v_u$ with initial conditions at v_u of (1,1). Note that in the last case, because we are interested in the voltage range $v > v_u$, the Dirac-delta function does not feature. Once these subsolutions are obtained κ can be extracted from the condition that $\hat{\jmath}^R(v_{th}) = 0$ so that $\kappa = -\hat{\jmath}^R(v_{th};0)/\hat{\jmath}^r(v_{th};1)$. This now gives the correct mix for the quantities $\hat{\jmath}^R(v)$ and $\hat{\jmath}_s^R(v)$. Given that their values at v_u are now known, equation pair (A8),(A9) can be integrated down from $v_u \to v_s$. This completes the derivation of the component proportional to $\hat{R}_s$.

Step 3. We now have the solutions for $\hat{\jmath}^R$ and $\hat{\jmath}^r$ over the full voltage range. At the stable fixed point v_s the flux $\hat{J}$ is zero. Hence, from the first of equation pair (A5) we have $0 = \hat{r}\hat{\jmath}^r(v_s) + \hat{R}_s\hat{\jmath}^R(v_s)$ so that $\hat{r} = -\hat{R}_s\hat{\jmath}^R(v_s)/\hat{\jmath}^r(v_s)$, which constitutes the numerical solution for the modulated rate.

3. General numerical solution of the master equation

Following similar approaches for leaky-integrate and fire models [28–32], the full system can be solved numerically by integrating the master equation, defined through the combination of Eqs. (3), (4), and (6). Again, it was found that a naive approach had poor convergence properties—here due to the long exponential tail in the distribution at high voltages. To avoid this a rescaling was sought that compressed the voltage range above v_T. The following transformation

$$z = \frac{e^{(v-v_T)/\delta_T} + v/v_T}{e^{(v-v_T)/\delta_T} + v/v_T + 1} \tag{A11}$$

combined with a fourth-order Runga-Kutta scheme generated accurate results with reasonable integration times. The transformation is monotonic, with the property that for $v < v_T$ the mapping is linear $z \sim v/v_T$, whereas in the limit of high voltages $z \to 1$. Hence the range of z is finite (between $\sim v_u/v_T$ and 1). It was also convenient to mollify the reset mechanism from a delta function to a Gaussian centered on v_{re} with a standard deviation (0.1 mV) that was sufficiently narrow such that its width did not affect the final result significantly but, nevertheless, mitigated the effects of the discontinuity in probability density on the integration scheme. This method was used to generate the response in Figs. 3(b) and 3(c).

4. Parameters used for the stimulation in Fig. 3

To illustrate the effect of the different high-frequency asymptotics in the time domain an input-rate stimulation $R_s(t)$ was constructed [see Fig. 3(a)] comprising the instantaneous switching from zero to a finite value after 5 ms, which can be considered as a model of the transition from a down state to an up state, three Gaussian pulses of decreasing duration but fixed area $g_1(t)$, $g_2(t)$, $g_3(t)$ that converge towards a Dirac δ-function impulse, a step rate increase followed by step decrease $s(t)$, and two chirps $c_1(t)$ and $c_2(t)$ of different frequency demonstrating that the high-frequency asymptotics are relevant even for transitory oscillatory input. The time t ran from $0 \to 570$ ms and was sampled at 2 μs.

Using case (i) as an example [Fig. 3(a), blue] we write

$$R_i(t) = \theta(t-5)[R_i + \gamma_i S(t)], \tag{A12}$$

where R_i is the steady-state input for case (i) of 2.1 kHz [see Fig. 1(c): $R_{ii} = 0.59$ kHz and $R_{iii} = 0.14$ kHz for cases (ii) and (iii)] and γ_i is a gain factor such that each of the cases will have the same late-time response to a weak step change in synaptic input rate around a 5 Hz steady-state output rate. This normalizes the response to slowly varying stimuli across cases (i)–(iii), ensuring a fair comparison of

the high-frequency response. Values were $\gamma_i = 0.025$ kHz, $\gamma_{ii} = 0.0126$ kHz, and $\gamma_{iii} = 0.0059$ kHz.

The shape function is common to each of the cases

$$S(t) = g_1(t) + g_2(t) + g_3(t) + s(t) + c_1(t) + c_2(t) \quad \text{(A13)}$$

with the components described above. Quantitatively, the three Gaussian pulses took the form

$$g_k(t) = 10 \exp\left[-(t - t_{gk})^2/2\sigma_{gk}^2\right]/\sqrt{2\pi}\sigma_{gk}, \quad \text{(A14)}$$

where $t_{g1} = 140$ ms, $t_{g2} = 190$ ms, and $t_{g3} = 240$ ms; $\sigma_{g1} = 1.7$ ms, $\sigma_{g2} = 0.85$ ms, and $\sigma_{g3} = 0.42$ ms to give full width half maxima of 4 ms, 2 ms, and 1 ms, respectively. The step change in rate took the form $s(t) = 2[\theta(t - t_{s1}) - \theta(t - t_{s2})]$, where $t_{s1} = 290$ ms and $t_{s2} = 350$ ms. Chirps were implemented by multiplying a cosine and a Gaussian

$$c_k(t) = \kappa_k \cos(2\pi f_k t) \exp\left[-(t - t_{ck})^2/2\sigma_{ck}^2\right], \quad \text{(A15)}$$

where $\kappa_1 = 5$ and $\kappa_2 = 7$, $t_{c1} = 445$ ms and $t_{c2} = 520$ ms, and $\sigma_{c1} = \sigma_{c2} = 10$ ms.

[1] M. N. Shadlen and W. T. Newsome, Curr. Opin. Neurobiol. **4**, 569 (1994).
[2] G. L. Gernstein and B. Mandelbrot, Biophys. J. **4**, 41 (1964).
[3] R. B. Stein, Biophys. J. **5**, 173 (1965).
[4] P. I. M. Johannesma, in *Neural Networks*, edited by E. R. Caianiello (Springer, New York, 1968), pp. 116–144.
[5] L. M. Ricciardi, *Diffusion Processes and Related Topics on Biology* (Springer-Verlag, Berlin, 1977).
[6] B. Lindner, L. Schimansky-Geier, and A. Longtin, Phys. Rev. E **66**, 031916 (2002).
[7] B. Lindner, A. Longtin, and A. Bulsara, Neural Comput. **15**, 1761 (2003).
[8] N. Brunel and V. Hakim, Neural Comput. **11**, 1621 (1999).
[9] G. Gigante, M. Mattia and P. Del Giudice, Phys. Rev. Lett. **98**, 148101 (2007).
[10] S. Song, P. Sjöström, M. Reigl, S. Nelson, and D. B. Chklovskii, PLoS Biol. **3**, e350 (2005).
[11] H. Markram, J. Lübke, M. Frotscher, A. Roth, and B. Sakmann, J. Physiol. **500**, 409 (1997).
[12] R. Perin, T. K. Berger, and H. Markram, Proc. Natl. Acad. Sci. U.S.A. **108**, 5419 (2011).
[13] A. Reyes and B. Sakmann, J. Neurosci. **19**, 3827 (1999).
[14] D. Contreras and M. Steriade, J. Neurosci. **15**, 604 (1995).
[15] M. V. Sanchez-Vives and D. A. McCormick, Nat. Neurosci. **3**, 1027 (2000).
[16] A. Destexhe, M. Rudolph, and D. Pare, Nat. Rev. Neurosci. **4**, 739 (2003).
[17] W. Bair, R. Zohary, and W. T. Newsome, J. Neurosci. **21**, 1676 (2001).
[18] M. R. DeWeese and A. M. Zador, J. Neurosci. **26**, 12206 (2006).
[19] T. Deniz and S. Rotter, J. Phys. A **50**, 254002 (2017).
[20] L. F. Abbott, J. A. Varela, K. Sen, and S. B. Nelson, Science **275**, 221 (1997).
[21] M. V. Tsodyks and H. Markram, Proc. Natl. Acad. Sci. U.S.A. **94**, 719 (1997).
[22] N. Hohn and A. N. Burkitt, Phys. Rev. E **63**, 031902 (2001).
[23] M. J. E. Richardson and W. Gerstner, Neural Comput. **17**, 923 (2005).
[24] L. Wolff and B. Lindner, Phys. Rev. E **77**, 041913 (2008).
[25] B. W. Knight, A. Omurtag, and L. Sirovich, Neural Comput. **12**, 1045 (2000).
[26] A. Kuhn, A. Aertsen, and S. Rotter, Neural Comput. **15**, 67 (2003).
[27] M. Helias, M. Deger, S. Rotter, and M. Diesmann, Front. Neurosci. **5**, 19 (2011).
[28] R. Iyer, V. Menon, M. Buice, C. Koch, and S. Mihalas, PLoS Comput. Biol. **9**, e1003248 (2013).
[29] D. Q. Nykamp and D. Tranchina, J. Comp. Neuro. **8**, 19 (2000).
[30] N. Cain, R. Iyer, C. Koch, and S. Mihalas, PLoS Comput. Biol. **12**, e1005045 (2016).
[31] E. Haskell, D. Q. Nykamp, and D. Tranchina, Netw.: Comput. Neural Syst. **12**, 141 (2001).
[32] C. Ly and D. Tranchina, Neural Comput. **21**, 360 (2009).
[33] Y. Ming Lai and M. de Kamps, Phys. Rev. E **95**, 062125 (2017).
[34] M. J. E. Richardson and R. Swarbrick, Phys. Rev. Lett. **105**, 178102 (2010).
[35] F. Droste and B. Lindner, J. Comput. Neurosci. **43**, 81 (2017).
[36] D. Angulo-Garcia, S. Luccioli, S. Olmi, and A. Torcini, New J. Phys. **19**, 053011 (2017).
[37] S. Olmi, D. Angulo-Garcia, A. Imparato, and A. Torcini, Sci. Rep. **7**, 1577 (2017).
[38] A. N. Burkitt, Biol. Cybern. **95**, 1 (2006).
[39] A. N. Burkitt, Biol. Cybern. **95**, 96 (2006).
[40] A. Hodgkin and A. Huxley, J. Physiol. **117**, 500 (1952).
[41] G. B. Ermentrout and N. Kopell, SIAM J. Appl. Math. **46**, 233 (1986).
[42] N. Fourcaud-Trocmé, D. Hansel, C. van Vreeswijk, and N. Brunel, J. Neurosci. **17**, 11628 (2003).
[43] L. Badel, S. Lefort, R. Brette, C. C. H. Petersen, W. Gerstner, and M. J. E. Richardson, J. Neurophysiol. **99**, 656 (2008).
[44] P. M. Harrison, L. Badel, M. J. Wall, and M. J. E. Richardson, PLOS Comput. Biol. **11**, e1004165 (2015).
[45] L. Badel, S. Lefort, T. K. Berger, C. C. H. Petersen, W. Gerstner, and M. J. E. Richardson, Biol. Cybern. **99**, 361 (2008).
[46] N. Fourcaud-Trocme and N. Brunel, J. Comput. Neurosci. **18**, 311 (2005).
[47] J. Bezanson, A. Edelman, S. Karpinski, and V. B. Shah, SIAM Rev. **59**, 65 (2017).
[48] See Supplemental Material at http://link.aps.org/supplemental/10.1103/PhysRevE.98.042405 for the Julia1.0 code generating Figs. 1–3.
[49] M. J. E. Richardson, Phys. Rev. E **76**, 021919 (2007).
[50] J. Touboul and R. Brette, Biol. Cybern. **99**, 319 (2008).
[51] M. Hausser and A. Roth, J. Neurosci. **17**, 7606 (1997).
[52] I. C. Kleppe and H. P. C. Robinson, Biophys. J. **77**, 1418 (1999).
[53] B. Naundorf, F. Wolf, and M. Volgushev, Nature (London) **440**, 1060 (2006).

[54] H. Koendgen *et al.*, Cereb. Cortex **18**, 2086 (2008).
[55] C. Boucsein, T. Tetzlaff, R. Meier, A. Aertsen, and B. Naundorf, J. Neurosci. **29**, 1006 (2009).
[56] W. Wei and F. Wolf, Phys. Rev. Lett. **106**, 088102 (2011).
[57] T. Tchumatchenko, A. Malyshev, F. Wolf, and M. Volgushev, J. Neurosci. **31**, 12171 (2011).
[58] T. Broicher *et al.*, J. Neurosci. **32**, 14374 (2012).
[59] V. Ilin, A. Malyshev, F. Wolf, and M. Volgushev, J. Neurosci. **33**, 2281 (2013).
[60] G. Eyal, H. D. Mansvelder, C. P. J. de Kock, and I. Segev, J. Neurosci. **34**, 8063 (2014).
[61] G. Testa-Silva *et al.*, PLoS Biol. **12**, e1002007 (2014).